COMMUNICATION

Check for updates

Decoupling manufacturing from application in additive manufactured antimicrobial materials†

Dominic J. Wales, [ID] ‡[a] Sara Miralles-Comins,§[b] Isabel Franco-Castillo,[c,d]
Jamie M. Cameron, [ID] [e] Qun Cao,[a] Erno Karjalainen,[a] Jesum Alves Fernandes, [ID] [f]
Graham N. Newton, [ID] [e] Scott G. Mitchell [ID] *[c,d] and Victor Sans [ID] *[b]

3D printable materials based on polymeric ionic liquids (PILs) capable of controlling the synthesis and stabilisation of silver nanoparticles (AgNPs) and their synergistic antimicrobial activity are reported. The interaction of the ionic liquid moieties with the silver precursor enabled the controlled *in situ* formation and stabilisation of AgNPs *via* extended UV photoreduction after the printing process, thus demonstrating an effective decoupling of the device manufacturing from the on-demand generation of nanomaterials, which avoids the potential aging of the nanomaterials through oxidation. The printed devices showed a multi-functional and tuneable microbicidal activity against Gram positive (*B. subtilis*) and Gram negative (*E. coli*) bacteria and against the mould *Aspergillus niger*. While the polymeric material alone was found to be bacteriostatic, the AgNPs conferred bactericidal properties to the material. Combining PIL-based materials with functionalities, such as *in situ* and photoactivated on-demand fabricated antimicrobial AgNPs, provides a synergistic functionality that could be harnessed for a variety of applications, especially when coupled to the freedom of design inherent to additive manufacturing techniques.

Introduction

Antimicrobial resistance is a significant global health challenge around the world.[1] A potential solution that has enjoyed significant interest are materials with inherent antimicrobial properties.[2] One example is silver nanoparticles (AgNPs), which exhibit broad antimicrobial potential,[3,4] and can be supported in a wide range of polymers and hydrogels.[5–8] Such materials can be fabricated into myriad functional shapes and devices by utilising the design freedoms afforded by 3D printing,[9] and indeed there are many examples of AgNP supporting materials that have been 3D printed.[10–17] Typically, the AgNPs are either dispersed in the resin before 3D printing, or the AgNPs are formed during the 3D printing process, and then the materials can be used immediately. However, the disadvantage to this approach is that it does not allow for tuneable fabrication of the AgNPs so the efficacy of the device is tailored for the particular application at the point of use.

Therefore, to maintain maximal antimicrobial efficacy, whilst still allowing for a responsive bespoke personalised healthcare approach enabled by the inherent freedoms afforded by 3D printing, decoupling of the manufacture of the 3D printed part and the formation of AgNPs is needed. There are some examples of 3D printed materials containing AgNPs, wherein the fabrication is decoupled from the AgNP formation, but they typically require post-printing treatments, like energy-intensive heating steps,[18] or immersion of the printed part in a reducing solution.[19]

A desirable alternative is a polymeric matrix that can be 3D printed, has the required mechanical properties and also maintains the silver precursor in the oxidised form to enable a controlled reductive formation of the AgNPs at the point of need. Fantino *et al.* have demonstrated on-demand photo-

[a]*Faculty of Engineering, University of Nottingham, University Park, Nottingham, NG7 2RD, UK*

[b]*Institute of Advanced Materials (INAM), Universitat Jaume I, 12071 Castellon, Spain. E-mail: sans@uji.es*

[c]*Instituto de Nanociencia y Materiales de Aragón (INMA-CSIC), CSIC-Universidad de Zaragoza, c/Pedro Cerbuna 12, 50009 Zaragoza, Spain*

[d]*CIBER de Bioingeniería, Biomateriales y Nanomedicina, Instituto de Salud Carlos III, 28029 Madrid, Spain. E-mail: scott.mitchell@csic.es*

[e]*GSK Carbon Neutral Laboratory, University of Nottingham, Jubilee Campus, Nottingham, NG8 2GA, UK*

[f]*School of Chemistry, University of Nottingham, University Park, Nottingham, NG7 2RD, UK*

reductive formation of AgNPs within photocured polyethylene glycol diacrylate (PEGDA), which was decoupled from the 3D printing step. However, their system appeared to offer limited ability to stabilise AgNPs, and nanoparticle aggregation and migration were observed.[20] One suitable class of materials to achieve superior stabilisation ability are poly(ionic liquids), also known as polymeric ionic liquids (PILs), which are poly-electrolytes,[21] formed from polymerisable ionic liquid mono-mers. PILs possess analogous properties to bulk ionic liquids in solution,[22,23] and also enable exquisite tuning of the polymer properties through a near-infinite combination of cations and anions, together with the broad range of architecture and morphology variations inherent to polymeric materials.[24] There are many examples of poly(ionic liquid) functional materials such as porous electro-optic films,[25] ion conductive polymer films,[26–29] dispersants,[30] and actuators.[31,32] Furthermore, PILs can also be 3D printed using a range of techniques, such as inkjet printing,[33] DLP,[34,35] and microstereolithography.[36] In addition, the ability of ionic liquids and PILs to stabilise and support metal nanoparticle precursor salts and nanoparticles has been well demonstrated.[37] Finally, ILs and PILs can be designed so as to possess inherent broad antimicrobial properties, against bacteria and fungi.[38–41]

Therefore, we propose the use of 3D printable poly(ionic liquids) to fabricate multifunctional materials that feature three key properties; (i) on-demand photoreductive formation of the AgNPs within the material that is decoupled from the 3D printing step; (ii) an antimicrobial effect of the PIL backbone; combined with (iii) the broad antimicrobial action afforded by AgNPs. Vat photopolymerisation is selected as the 3D printing technique for proof of concept, since it allows the rapid formulation of polymerisation formulations and the generation of precise, complex geometries.

Herein we report the development of novel 3D-printable materials based on two different polymeric ionic liquids (PILs) functionalised with silver nanoparticles (AgNPs), we compare and contrast the formation and stabilisation of the silver nanoparticles in the two formulations and investigate the antimicrobial properties. The ability of each PIL to stabilise active nanomaterials *via* photoreduction is demonstrated by effective decoupling of the fabrication from the on-demand generation of low polydispersity AgNPs by subsequent exposure to UV irradiation. Furthermore, the tuneable antimicrobial activity of the AgNP@PIL printed devices against Gram-positive *Bacillus subtilis* (*B. subtilis*) and Gram-negative *Escherichia coli* (*E. coli*) bacteria, and *Aspergillus niger* (*A. niger*) and *Cladosporium cladosporioides* (*C. cladosporioides*) fungi is presented.

Results and discussion

In this work, several formulations based on combinations of different IL based monomers (mIL) and cross-linkers were investigated (Fig. 1A & B), with the aim of developing an optimised ink composition for printing AgNP@PIL materials.

Initial 3D printing experiments used the digital light processing (DLP) technique, employing a Little RP printer with a DLP projector to generate the UV light required for polymerisation. Latter 3D printing experiments were performed with a newer liquid crystal display (LCD) based printer (Elegoo Mars). The latter allowed for marginally better resolution, and had a smaller footprint, but no differences for the printing process were noticed. The first tunable 3D printing ink formulation was based on the polymerisable monomeric IL (mIL) precursor 1-butyl-3-vinylimidazolium bis(trifluoromethane)sulfonimide ([BVIM][NTf$_2$]) (**mIL1**, Fig. 1A), which was synthesised from 1-butyl-3-vinylimidazolium bromide ([BVIM][Br]) *via* anion metathesis as described in the ESI.† [34,35] **mIL1** was chosen as the polymerisable ionic liquid component as it has been previously demonstrated as a suitable poly(ionic liquid) (PIL) for stabilising and solubilising hybrid organic–inorganic polyoxometalates, and forms mechanically resistant polymers when 3D printed.[34,35] Based on our previous experience, the initial ink formulation (**PIL1**, Fig. 1B) consisted of **mIL1** (80 mol%), the crosslinker 1,4-butanediol diacrylate (20 mol%) and the organic photoinitiator diphenyl(2,4,6-trimethylbenzoyl)phosphine oxide (TMDPO, 1 mol%) and was a clear, very pale yellow viscous liquid. This ink composition was chosen as it was previously found to be the most effective for 3D-printing of PILs with the DLP technique. To this baseline formulation silver hexafluoroantimonate (AgSbF$_6$, ~1 wt%) salt was solubilised and stabilised.

The photopolymerisation of the **PIL1** formulation resulted in well-defined clear and very pale yellow PIL parts (Fig. 2A, 0 min). The pale-yellow colour of the 3D printed **PIL1** pieces is attributed to the polymer, thus suggesting that the encapsulated silver was still in the Ag$^+$ state, despite exposure to the light during the 3D printing step. Furthermore, the UV-Visible spectra of the as printed pieces confirmed the absence of an absorption peak in the region $\lambda \approx 375$–475 nm, attributable to the LSPR band of the AgNPs (Fig. S1†),[42] but does show the expected absorption peak features for the photoinitiator TMPDO.[43] Then upon exposure to UV light, the photoreduction of Ag$^+$ to Ag(0) was initiated and the colour of the printed parts changed over time to increasingly darker shades of amber (Fig. 2A), and TEM analysis confirmed the presence of AgNPs (Fig. 2A, inset). The presence of Ag(0) was further confirmed by XPS characterisation, which revealed the expected peaks in the spectrum for Ag 3d$_{3/2}$ and Ag 3d$_{5/2}$ (Fig. S2†).[44] Indeed, the slight asymmetry of the Ag 3d$_{5/2}$ peak toward higher binding energies could be due to a convoluted peak that corresponds to aggregated Ag nanoparticles, which further corroborates the presence of AgNPs.[45]

Mechanical analysis of parts exposed to UV photoreduction for different times indicated an increase in tensile stiffness with increasing UV exposure time (Fig. S2B†). Additionally, the corresponding tan∂ *vs.* temperature curves revealed the T_g values (defined as the *x*-axis values at each curve maximum) also increased with increasing UV exposure time (Fig. 2B), the secondary peak at low temperatures can be attributed to local chain motions or side group movements in the polymer
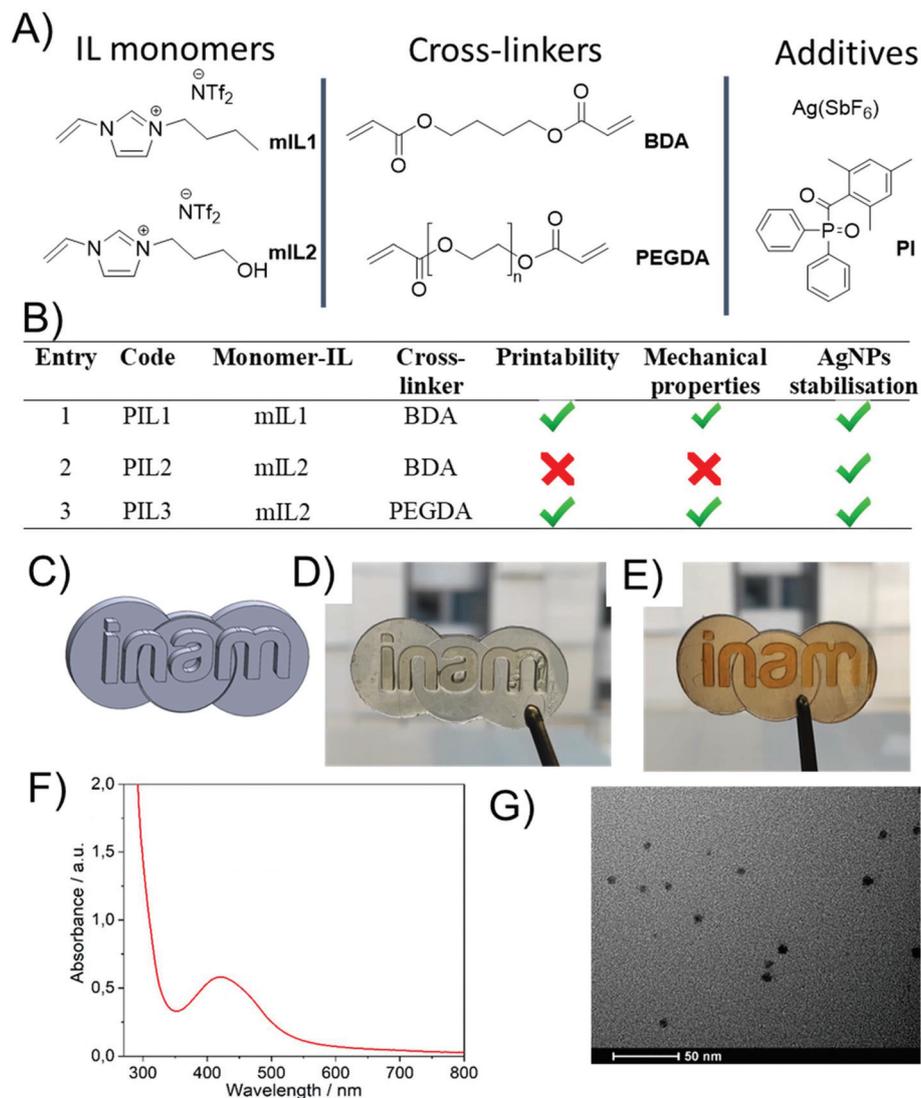
Fig. 1 This figure provides an overall visual summary of the work in this paper, and also shows the following specific results: (A) The components employed for the development of the 3D printable PIL-based formulations; (B) table summarising the formulations explored and a qualitative assessment of the properties of the materials developed. Unless indicated otherwise, 80 : 20 mol : mol, 1 mol% PI, 1 wt% AgSbF$_6$; (C) example CAD design that was employed as a benchmark for 3D-printing; (D) 3D-printed part with **PIL3** formulation without Ag reduction; (E) 3D printed part with **PIL3** formulation with AgNPs generated by post printing UV irradiation. Printed part; (F) the UV-Visible peak feature attributed to the AgNP plasmon in 3D-printed and UV-exposed **PIL3** centred at 422 nm; and (G) transmission electron micrograph of a 3D printed and UV-exposed **PIL3** part showing the presence of AgNPs dispersed within the PIL matrix.

chains.[46] The mechanical properties of the **PIL1** pieces are summarised in Fig. S2D.† FT-IR studies during UV exposure over time revealed only a small decrease in the intensity of the C=C stretch peak at ~1660 cm^{-1} after 5 minutes of UV exposure, and no further change upon further UV exposure (Fig. 2C). The peak feature at ~1660 cm^{-1} can also be attributed to the C=C bond in the imidazole ring,[47–49] and thus the intensity of this peak would not change upon further UV exposure. Therefore, it is proposed that the increase in tensile stiffness and T_g upon increased UV exposure time is due to the continued formation of AgNPs and/or aggregation of AgNPs, both of which contribute to modifying the mechanical pro-

perties of polymer matrices.[50] UV-Vis transmission spectroscopy experiments during the UV post-printing treatment further confirmed the formation of AgNPs due to the presence of a shoulder peak centred at $\lambda \approx 450$ nm increasing in absorbance, which is attributed to the AgNP plasmon. For comparison, an analogous liquid IL homogeneous system was prepared, where Ag(SbF$_6$) (1 wt%) was added to non-polymerisable 1-butyl-3-methylimidazolium bis(trifluoromethane)sulfonimide and photo-reduced under UV light ($\lambda = 395$ nm). In this case, the plasmon arising due to the presence of AgNPs, was also observed as a shoulder in the UV-Vis spectrum (see Fig. S3†). Interestingly, changing the monomer to 1-(3-hydroxy-
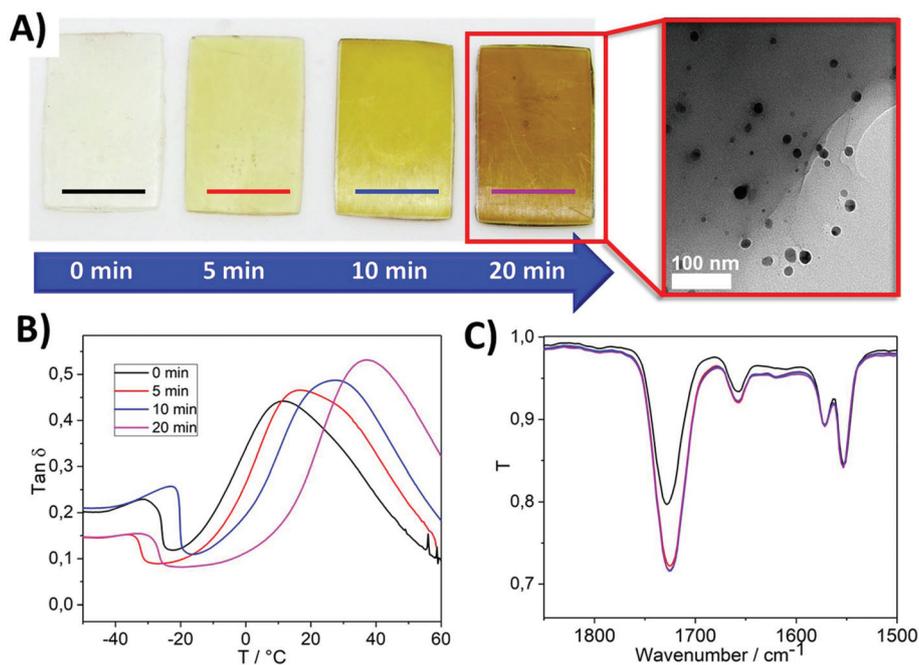
Fig. 2 (A) The **PIL1** 3D printed parts exhibited different colours depending on the exposure time to UV light (λ = 395 nm, 36 W, r.t.) with (red inset) a transmission electron micrograph showing the presence of nanoparticles; (B) The tan ∂ vs. temperature curves, where the T_g values (defined as the x-axis values at each curve maximum) increase with increasing UV exposure time; and (C) FT-IR spectrum demonstrating little to no change in the C=C peak upon increasing UV exposure time (the curve colours are the same as per the legend inset in (B). This suggests that further polymerisation of unpolymerised C=C bonds in the materials is not contributing to the increases in tensile stiffness and T_g upon UV exposure.

propyl)-3-vinylimidazolium bis(trifluoromethane)sulfonimide [POHVIm][NTf$_2$] (**mIL2**, Fig. 1B) in the formulation, whilst keeping the rest of the formulation constant (**PIL2**), led to better resolved plasmons after post-curing with a well-defined plasmon (distinct absorption peak, rather than a shoulder feature) with a maximum at λ = 413 nm (Fig. S4,† blue curve).

However, it was determined that LCD-based printing of the **PIL2** formulation resulted in excessively rigid samples, which deformed and cracked during the polymerisation process. It was hypothesised that the presence of the hydroxyl group of the cation, combined with the use of 1,4-BDA as cross-linking agent, had an influence on the mechanical properties of the resulting material, which in turn affected the printability. Instead, use of poly(ethyleneglycol) diacrylate (PEGDA, M_n = 575 g mol^{-1}) resulted in much more flexible films (herein **PIL3**, Fig. 1B), which showed suitable mechanical properties for the polymerisation and 3D printing of suitable geometries with acceptable resolution (Fig. 1C–E and Fig. S5†). The corresponding UV-Visible peak feature attributable to AgNPs was well-defined and centred at 422 nm (Fig. 1F and Fig. S4,† red curve) and the AgNPs were well dispersed within the PIL matrix (Fig. 1G). Now that a suitable composition of PIL ink had been determined, aging experiments were performed to determine the stability of the AgNP@PIL parts over time.

To examine the photostability of the AgNP@PIL materials, **PIL2** 3D-printed parts were stored either under ambient lighting or in dark conditions. It was observed that AgNP@**PIL2** materials, which had been generated by post-curing photore-

duction exhibited photo-aging when exposed to ambient light in terms of an increase in the magnitude of the absorbance peak attributed to AgNPs, suggesting the continued photoreductive formation of AgNPs (Fig. S6†). The stability of 3D-printed AgSbF$_6$-containing PILs to photoreduction was then investigated and it was determined that storage in dark conditions was required to prevent photo-aging. When non-photoreduced **PIL2** pieces were exposed to three weeks of ambient light a peak (centred at ~450 nm) in the UV-Visible transmission spectra developed, suggesting the formation of AgNPs (Fig. 3A). In contrast, non-photoreduced 3D printed **PIL2** pieces stored in the dark produced no such observable absorbance feature that could be attributed to AgNPs (Fig. 3B). Thus, for use of these materials as potential antimicrobial materials/devices, storage in dark conditions demonstrates the hypothesis that it is possible to decouple the manufacturing of devices by 3D printing from the photoreduction of active AgNPs.

The presence of hydrophobic poly(ionic liquids) combined with AgNPs make PILs interesting and highly applicable candidates for antimicrobial surface coatings to prevent biofilm formation. Ionic liquids are gaining relevance as they present some desirable characteristics highly relevant in the clinical use, such as improved bacterial resistance, antibiofilm properties, and the possibility of being 3D-printed as specific dental objects, among others.[41,51] The antimicrobial activity of the PILs reported herein were evaluated against non-pathogenic *E. coli* and *B. subtilis* and two moulds (*A. niger* and
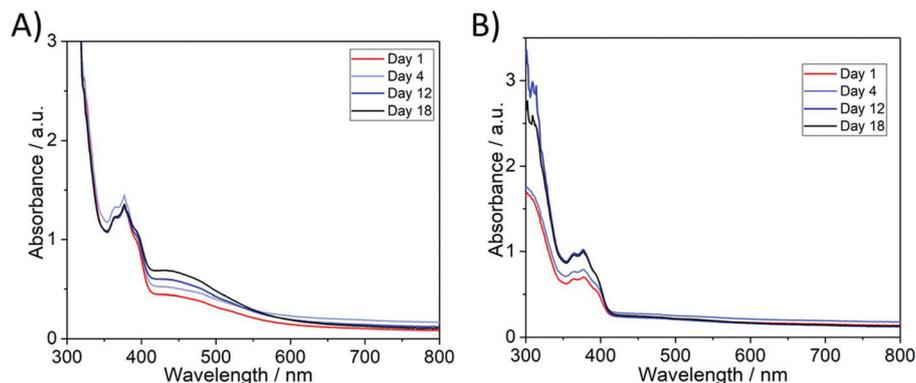
Fig. 3 (A) AgNPs@**PIL2** non-reduced and then aged under ambient light highlighting the development of a peak feature at ~450 nm suggesting the formation of AgNPs; and (B) AgNPs@**PIL2** non-reduced and then aged under dark conditions, showing no AgNP plasmon. In all cases the samples were exposed to ambient atmosphere.

C. cladosporioides) *via* zone of inhibition (Kirby-Bauer) tests and cell proliferation assays, as well as biofilm inhibition studies. In general, PIL and AgNP@PIL samples act to inhibit microbial growth, but AgNP-containing PILs (AgNP@PIL) are more effective at reducing bacterial viability.

In the first instance, a zone of inhibition test of **PIL1** and AgNPs@**PIL1** revealed that only the AgNP@**PIL1** displayed an inhibition halo against *E. coli* and *B. subtilis* (Fig. 4A). This inhibition of bacterial growth around the sample is due to the diffusion of the Ag$^+$ ions into the agar, which is the most important factor in the antimicrobial activity of the AgNPs against bacteria.[51] No inhibition halo was found with the **PIL1** samples due to the lack of silver. A delay halo—characterised for the mycelium growth but a lack of sporulation—was found around AgNP@**PIL1** incubated in the plate inoculated with *A. niger*. No inhibition nor delay halo was found with the **PIL1** sample, and neither **PIL1** nor AgNP@**PIL1** resulted in mycelium or sporulation inhibition for *C. cladosporioides* (Fig. 4B).

In order to determine the antibacterial activity of the samples in solution, the bacterial growth in cell culture media in the presence of the samples was monitored by optical density. **PIL1** repressed the growth of *E. coli* and *B. subtilis* in

Fig. 4 (A) Zone of Inhibition test of **PIL1** and AgNPs@**PIL1** against two bacterial strains (*E. coli* and *B. subtilis*) and (B) two moulds (*A. niger* and *C. cladosporioides*).

liquid media over a 24 hour period but, interestingly, the corresponding reduction in bacterial cell viability was lower for the Gram-positive *B. subtilis* (Fig. 5A). Since hydrophobic antimicrobial compounds often act by disrupting, depolarising, and destabilising bacterial cell membranes,[52,53] our hypothesis was that the bacteriostatic PIL samples and the associated stress to the cell membrane provokes increased proliferation in this species. Furthermore, *B. subtilis* can form protective endospores that are able to tolerate harsh environmental conditions, thus another hypothesis is that the presence of the PIL without silver can stimulate the production of endospores by *B. subtilis*, potentially explaining the differences compared with the growth of *E. coli*. This was confirmed by Environmental Scanning Electron Microscopy (ESEM), which showed a high degree of sporulation in *B. subtilis* (Fig. 5C). On the other hand, the AgNPs@**PIL1** variant was found to reduce bacterial cell growth of *E. coli* and *B. subtilis* by 86% and 75%, respectively, as expected, due to the antimicrobial effect of silver. Broth and agar dilution methods are standard methods used to determine the antimicrobial effect of the compounds, but these assays are standardised for soluble compounds. Hence, performing a surface antimicrobial assay is essential when using compounds which are meant to be applied as a coating or, like in this case, they are created directly as a 3D object. Here, a modified Japanese Industrial Standard Z 2801 method was used to determine the surface antimicrobial activity of **PIL1** and AgNP@**PIL1** (Table 1). **PIL1** displayed a bacterial reduction of 100% and 89% for *E. coli* and *B. subtilis*, respectively, while AgNP@**PIL1** reduced 100% of the bacterial cell count. Subcultures of the supernatants confirmed the bactericidal effect of the AgNP@**PIL1**, while **PIL1** only displayed bactericidal effect against *E. coli*. These results are commensurate with the results in liquid medium and the ESEM images (Fig. 5A), where the samples containing Ag displayed a higher antimicrobial effect, with *B. subtilis* being the most resistant strain. The differences in antimicrobial activity between the solution and the surface activity tests show that the antimicrobial properties are based primarily on surface contact-
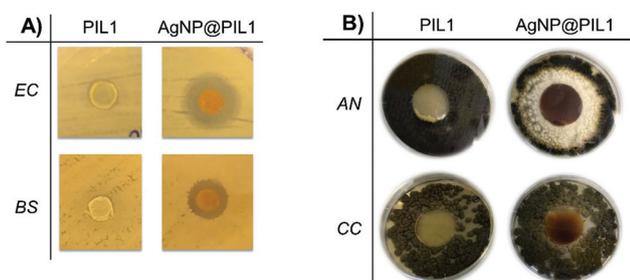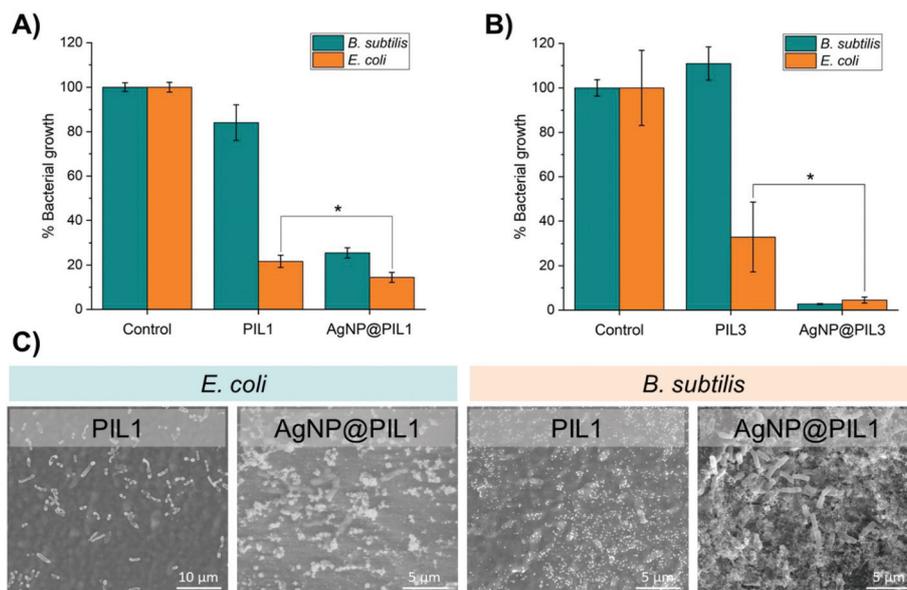
Fig. 5   (A) Bacterial cell viability of *E. coli* and *B. subtilis* incubated with **PIL1** and AgNP@**PIL1** and (B) **PIL3** and AgNP@**PIL3**. (C) ESEM images of **PIL1** and AgNP@**PIL1** inoculated with *E. coli* and *B. subtilis*. Both **PIL1** and AgNP@**PIL1** affect *E. coli* morphology, disrupting the cell membrane. On the other hand, **PIL1** stimulates *B. subtilis* sporulation, while the AgNP@**PIL1** prevents colonisation of the polymeric surface due to a higher bactericidal effect.

Table 1   Bacterial reduction (%) after 24 hours incubation over the samples

	Bacterial reduction	
	E. coli	*B. subtilis*
PIL1	100%	89%
AgNP@**PIL1**	100%	100%

killing rather than the release of an active component, such as Ag⁺ ions, into the local environment.[51] Evaluation of the anti-bacterial activity of the **PIL3** formulation yielded similar results, however, AgNP@**PIL3** was found to possess the highest degree of inhibition after 24 hours of incubation, resulting in a reduction of around 95% for both bacterial strains (Fig. 5B).

Conclusions

Herein, the capability of novel 3D-printed materials consisting of polymeric ionic liquids (PILs) for the controlled on-demand synthesis, and subsequent stabilisation, of silver nanoparticles (AgNPs) has been demonstrated. It was determined that the nature of the ionic liquid moieties affected the *in situ* formation of the AgNPs and enabled the controlled formation and stabilisation of AgNPs *via* extended UV photoreduction after the 3D printing process. This demonstrated an effective decoupling of the 3D printing fabrication step from the on-demand generation of AgNPs with narrow size dispersity by subsequent exposure to UV irradiation. Upon further investigation, it was determined that the structure of the cation of the monomer ionic liquid had a profound effect on the formation of AgNPs, with a discrete UV-Vis peak feature attributed to the plasmon resonance of well-formed discrete AgNPs within the PILs formed from **mIL2** (AgNPs@**PIL3**), in contrast to a broad shoulder feature measured in the UV-Vis spectrum of AgNPs@**PIL1**. Thus, through careful choice of monomer ionic liquid, a suitable crosslinker for favourable mechanical properties, and a formulation that had previously been shown to be effective for 3D printing, the fabrication of materials/devices decoupled from on-demand photo-reductive formation of AgNPs for enhanced antimicrobial activity was realised. Indeed, the printed devices showed a multi-functional and tuneable microbiocidal activity against Gram positive (*B. subtilis*) and Gram negative (*E. coli*) bacteria and against the fungus *A. niger*. PIL-based materials were found to be bacteriostatic, whereas AgNPs@PIL materials possessed enhanced antimicrobial activity and bactericidal properties against the tested strains.

This work represents the first example of the novel combination of the decoupled *in situ* photoreductive fabrication of silver nanoparticles from the fabrication *via* 3D printing of the PIL-based materials. This *in situ* generation of nanostructured antimicrobial materials opens new routes to the development of 3D printed devices resistant to biofilm formation, for applications in the biomedical, food technology and healthcare industries. Furthermore, the near infinite combinations of cations and anions possible in PIL-based materials allows for further tuning and enhancement of the synergistic antimicrobial properties, especially when combined with the freedom of design inherent to additive manufacturing techniques.

Experimental and methods

General experimental information

Unless otherwise stated, all reagents were purchased from Sigma-Aldrich and used without further purification. BDA (90%) and 1-vinylimidazole were used after purification by passing through a short column of basic alumina (aluminium oxide).

The 3D printers used in this study were a LittleRP 3D printer and an Elegoo Mars. The Little RP 3D printer was equipped with an Acer P1500 projector (3D printer light source) that was fitted with an OSRAM P-VIP high pressure (>200 bar) Hg vapour lamp (210 W). The Elegoo Mars printed was equipped with a 2560 × 1440 2 K HD masking LCD, illuminated with 40 W UV LED backlight (λ = 405 nm). The light sources in both printers were both ∼3000 lumens. UV–vis spectra were collected using an Agilent Cary 5000 UV–vis–NIR spectrophotometer. FT-IR spectra were collected on a Bruker Alpha fitted with a Platinum ATR module. ^{1}H NMR spectra were recorded on a Bruker AVX400 (400 MHz) spectrometer at ambient temperature. ^{13}C NMR spectra were recorded on a Bruker AVX400 (101 MHz) spectrometer at ambient temperature. Environmental Scanning Electron Microscopy (ESEM) data was collected on a Quanta FEG-250 (FEI Company) field emission SEM for high-resolution imaging working in ESEM mode using a GSED detector under high relative humidity conditions. Transmission electron microscopy (TEM) measurements were performed using a JEOL 2000-FX operated with an accelerating voltage of 200 kV. The samples were prepared using ultramicrotomy process, where sample slices of few nanometres thickness were deposited on TEM grids. The mechanical analyses were performed with a TA Q800 DMA using a tension clamp. The moduli measurements as a function of temperature were measured using a strain amplitude of 0.1% and frequency of 1 Hz. The samples were cooled to −50 °C and stabilised at −50 °C for 5 min. Finally, the sample was then heated to 200 °C at the rate of 5 °C min^{-1}. The moduli were measured during the heating run. For the stress–strain measurements, the samples were first equilibrated at 25 °C for 5 min and then the force was ramped from 0 to 18 N at the rate of 1 N min^{-1} and the stress–strain curves were recorded.

Synthesis of ionic liquids

Full synthesis details and characterisation data are given at the end of the ESI.†

Process for 3D printing imidazolium PIL networks

The process for 3D printing imidazolium PIL pieces fabricated with 80 mol% [BVIM][NTf$_2$] (**mIL1**) ionic liquid is given as an example. The stereolithography fabrication began by slicing a 3D computer aided design model into individual images for projecting onto the photocurable ink. Additive manufacturing software, Creation Workshop RC36, was used to create slices of a desired thickness (50 μm per layer), control the projection time of the images by the projector, and the movement of the

build plate of the LittleRP FlexVat. For the Elegoo Mars 3D printer CHITUBOX software was employed. Then the printer vat was filled with the premixed **PIL1** ink, which contained 80 mol% [BVIM][NTf$_2$], 20 mol% 1,4-butanediol diacrylate (BDA), 1 mol% diphenyl(2,4,6-trimethylbenzoyl)phosphine oxide (photoinitiator) and 1 wt% silver hexafluoroantimonate (AgSbF$_6$). Then the build plate was lowered into the ink against the transparent film of the bottom of the vat. The software then controlled the projector to show a black background with white images of each of the layers which were to be photo-cured. The UV light passed through the transparent bottom of the vat. Each layer (50 μm) was cured for 8 s. After 8 s, the printer showed a black background (negligible light was projected into the photocurable ink) whilst the build plate was automatically lifted by 50 μm. Then the software loaded the image of the next layer and turned "on" the UV light by showing the next white colour image. This process was repeated until the object was completely fabricated. After the object was fabricated, the object was isolated and copiously washed with isopropyl alcohol to remove any uncured ink.

UV–Vis absorbance measurements of 3D-printed pieces

For collection of the UV–vis absorbance spectra of the 3D printed specimen, before and after irradiation with UV light, the specimen was first affixed to a metal holder exposed to UV light for a determined fixed amount of time, then a UV–vis spectrum of this specimen was collected using the Cary 5000 UV–vis–NIR spectrophotometer. Once the UV-Vis spectrum was collected, the procedure was repeated until a total UV light exposure of the desired time was reached.

Microorganisms and growth conditions

Two bacterial strains were tested in the antibacterial assays: *Escherichia coli* DH5α as a Gram-negative model and *Bacillus subtilis* 1904-E as a Gram-positive model. Two moulds from the "Colección Española de Cultivos Tipo (CECT)" were tested in the antifungal assays: *Aspergillus niger* CECT 2088 and *Cladosporium cladosporioides* CECT 2111. Fungal spore suspensions were stored in 0.1% Tween, 20% glycerol at −80 °C prior to use. The following culture media was used: Tryptone Soy Agar (TSA) (Thermo Scientific™), Sabouraud Dextrose Agar supplemented with chloramphenicol (SDA) (Scharlab, S. L.), as solid media; Luria–Bertani (LB) and Nutrient Broth (NB) (Scharlab, S. L.) as liquid media. The microbial growth conditions are summarised in the Table 2.

Agar diffusion test

A modified Kirby Bauer disk diffusion technique was used. The 3D printed samples (3 mm-diameter circles of PIL and AgNPs@PIL) were first sterilised with ethanol 70% and then they were placed in solid media previously inoculated with a bacterial lawn (10^7 CFU mL^{-1}) of *E. coli* or *B. subtilis*. After 24 hours of incubation at 37 °C, the inhibition halo around the samples was observed.

For the antifungal assay, the 3D printed samples (20 mm-diameter circles of PIL and AgNPs@PIL) were sterilised with

Table 2 Microorganisms and growth conditions

Microorganism		Solid medium	Liquid medium	Incubation temperature (°C)	Pre-inoculum incubation
Bacteria	*E. coli* DH5α	TSA	LB	37	24 hours
	B. subtilis	TSA	NB	37	24 hours
Fungi	*A. niger*	SDA	—	35	4 days
	C. cladosporioides	SDA	—	25	4 days

ethanol 70% and then placed in solid media previously inoculated with a spore solution (10^4 conidia mL^{-1}) of *A. niger* or *C. cladosporioides*. After 96 hours of incubation at the corresponding temperature (see Table 2), the inhibition halo around the samples was observed.

Bacterial cell proliferation assay

Bacterial growth was recorded measuring the optical density (OD) of the samples at 600 nm over a 24 hour period using a microplate reader (Thermo Scientific MULTISKAN GO). Results were compared with the OD variation of a control culture containing only *E. coli* or *B. subtilis*. The data for all control experiments and antibacterial assays are based on a total of six repeats to verify the reproducibility of the results and to calculate the mean values and the standard deviation; each experiment was repeated a minimum of three times to verify the results between different inoculations. The samples (PIL and AgNPs@PIL), previously sterilised with ethanol 70%, were placed in a 24-well plate inoculated with 1 mL of the inoculum (1×10^7 CFU mL^{-1} of *E. coli* or *B. subtilis*), incubated at 37 °C, and the antiproliferative effects induced by the samples were observed by plotting optical density (OD) *vs.* time. Bacterial growth was recorded measuring the optical density (OD) of 100 μL collected from each well of the 24-well plate, in a 96-well plate. Measurements at 600 nm were performed using a microplate reader, each hour during the first 8 hours and at 24 hours as a final point. To maintain the final volume (1 mL) during the experiment, the 100 μL subtracted from the wells from the 24-well plate were replaced with 100 μL of medium. Results were compared with the OD variation of a control culture containing only bacteria (*E. coli* or *B. subtilis*). Statistical analysis was performed using unpaired *t*-test. *P* values <0.05 were considered significant. Single stars denote $0.01 < P < 0.05$.

Surface antimicrobial activity

The surface antimicrobial activity was studied using a modified JIS Z 2801 standard. The protocol lasts three days. On the first day, a bacterial suspension of 1×10^7 CFU mL^{-1} was prepared and then 50 μL of this suspension was added over the surface of the samples of interest (2×2 cm) and over a reference sample with no antimicrobial activity (2×2 cm) after the sterilisation of these samples with ethanol 70%. In order to even the contact surface, a coverslip was put above the 50 μL of bacterial suspension in all the samples. The samples were incubated in a humid chamber at 37 °C for 24 h. After the 24 h of incubation, the bacteria over the samples were extracted

into liquid medium by putting the samples into a 50 ml falcon with 15 mL of culture media and shaking them one minute with a vortex. The culture media with the extracted bacteria was then diluted and sown in agar plates, which were incubated at 37 °C during 24 h. On the last day, the CFU of the cultivated agar plates were counted. The percentage of bacterial log reduction was obtained using the following formula:

$$\text{Reduction} = \log(\text{cfu reference sample}) - \log(\text{cfu antimicrobial sample})$$

Environmental scanning electron microscopy (ESEM) of the bacteria incubated over the samples

The effect of the samples (PIL and PIL@AgNPs) on the morphology of the bacteria was studied by ESEM. The samples were sterilised with ethanol 70% and inoculated with 100 μL of a 10^4 CFU mL^{-1} bacterial suspension. Then the inoculated samples were incubated in a humid chamber at 37 °C for 24 h. After the incubation time, the samples were rinsed with distilled sterile water and visualised on a Quanta FEG-250 (FEI Company) field emission SEM for high-resolution imaging working in ESEM mode using a GSED detector.

Conflicts of interest

There are no conflicts to declare.

Acknowledgements

Microscopias Avanzadas (LMA) at Universidad de Zaragoza for offering access to their instruments and expertise.

References

1 J. M. A. Blair, M. A. Webber, A. J. Baylay, D. O. Ogbolu and L. J. V. Piddock, *Nat. Rev. Microbiol.*, 2015, **13**, 42–51.

2 S. Mahira, A. Jain, W. Khan and A. J. Domb, in *Antimicrobial Materials for Biomedical Applications*, Royal Society of Chemistry, 2019, pp. 1–37, DOI: 10.1039/9781788012638-00001.

3 T. C. Dakal, A. Kumar, R. S. Majumdar and V. Yadav, *Front. Microbiol.*, 2016, **7**, 1831.

4 M. B. Estevez, S. Raffaelli, S. G. Mitchell, R. Faccio and S. Alborés, *Molecules*, 2020, **25**, 2023–2023.

5 N. Karak, in *Nanomaterials and Polymer Nanocomposites*, ed. N. Karak, Elsevier, 2019, pp. 47–89.

6 B. Tylkowski, A. Trojanowska, M. Nowak, L. Marciniak and R. Jastrzab, *Phys. Sci. Rev.*, 2017, **2**, 0024.

7 C. C. Piras, C. S. Mahon and D. K. Smith, *Chem. – Eur. J.*, 2020, **26**, 8452–8457.

8 Y. Niu, T. Guo, X. Yuan, Y. Zhao and L. Ren, *Soft Matter*, 2018, **14**, 1227–1234.

9 I. Gibson, D. W. Rosen and B. Stucker, *Additive Manufacturing Technologies: Rapid Prototyping to Direct Digital Manufacturing*, Springer-Verlag US, Boston, MA, U. S., 2010.

10 F. Afghah, M. Ullah, J. S. M. Zanjani, P. A. Sut, O. Sen, M. Emanet, B. S. Okan, M. Culha, Y. Menceloglu and M. Yildiz, *Biomed. Mater.*, 2020, **15**, 035015.

11 C. Bergonzi, G. Remaggi, C. Graiff, L. Bergamonti, M. Potenza, M. C. Ossiprandi, I. Zanotti, F. Bernini, R. Bettini and L. Elviri, *Nanomaterials*, 2020, **10**, 844.

12 S. Chen, J. Yang, Y.-G. Jia, B. Lu and L. Ren, *Materials*, 2018, **11**, 2444.

13 D. Podstawczyk, D. Skrzypczak, X. Połomska, A. Stargała, A. Witek-Krowiak, A. Guiseppi-Elie and Z. Galewski, *Polym. Compos.*, 2020, **41**, 4692–4705.

14 M. Shin, K. H. Song, J. C. Burrel, D. K. Cullen and J. A. Burdick, *Adv. Sci.*, 2020, **6**, 1901229.

15 G. Taormina, C. Sciancalepore, F. Bondioli and M. Messori, *Polymers*, 2018, **10**, 212.

16 N. Vidakis, M. Petousis, E. Velidakis, M. Liebscher and L. Tzounis, *Biomimetics*, 2020, **5**, 42.

17 Y. Yagci, M. Sangermano and G. Rizza, *Polymer*, 2008, **49**, 5195–5198.

18 E. Fantino, A. Chiappone, F. Calignano, M. Fontana, F. Pirri and I. Roppolo, *Materials*, 2016, **9**, 589–589.

19 Z. Wu and Y. Hong, *ACS Appl. Mater. Interfaces*, 2019, **11**, 33734–33747.

20 E. Fantino, A. Chiappone, I. Roppolo, D. Manfredi, R. Bongiovanni, C. F. Pirri and F. Calignano, *Adv. Mater.*, 2016, **28**, 3712–3717.

21 D. Mecerreyes, *Prog. Polym. Sci.*, 2011, **36**, 1629–1648.

22 J. Dupont, *J. Braz. Chem. Soc.*, 2004, **15**, 341–350.

23 V. Sans, N. Karbass, M. I. Burguete, V. Compañ, E. García-Verdugo, S. V. Luis and M. Pawlak, *Chem. – Eur. J.*, 2011, **17**, 1894–1906.

24 W. Qian, J. Texter and F. Yan, *Chem. Soc. Rev.*, 2017, **46**, 1124–1159.

25 J. Huang, C.-a. Tao, Q. An, W. Zhang, Y. Wu, X. Li, D. Shen and G. Li, *Chem. Commun.*, 2010, **46**, 967–969.

26 M. G. Cowan, M. Masuda, W. M. McDanel, Y. Kohno, D. L. Gin and R. D. Noble, *J. Membr. Sci.*, 2016, **498**, 408–413.

27 J.-S. Lee, K. Sakaushi, M. Antonietti and J. Yuan, *RSC Adv.*, 2015, **5**, 85517–85522.

28 S. Washiro, M. Yoshizawa, H. Nakajima and H. Ohno, *Polymer*, 2004, **45**, 1577–1582.

29 S. Sen, S. E. Goodwin, P. V. Barbará, G. A. Rance, D. Wales, J. M. Cameron, V. Sans, M. Mamlouk, K. Scott and D. A. Walsh, *ACS Appl. Polym. Mater.*, 2021, **3**, 200–208.

30 Y. Biswas, T. Maji, M. Dule and T. K. Mandal, *Polym. Chem.*, 2016, **7**, 867–877.

31 Q. Zhao, J. W. C. Dunlop, X. Qiu, F. Huang, Z. Zhang, J. Heyda, J. Dzubiella, M. Antonietti and J. Yuan, *Nat. Commun.*, 2014, **5**, 4293.

32 Q. Zhao, J. Heyda, J. Dzubiella, K. Täuber, J. W. C. Dunlop and J. Yuan, *Adv. Mater.*, 2015, **27**, 2913–2917.

33 E. Karjalainen, D. J. Wales, D. H. A. T. Gunasekera, J. Dupont, P. Licence, R. D. Wildman and V. Sans, *ACS Sustainable Chem. Eng.*, 2018, **6**, 3984–3991.

34 V. G. Maciel, D. J. Wales, M. Seferin and V. Sans, *J. Cleaner Prod.*, 2019, **214**, 29–40.

35 D. J. Wales, Q. Cao, K. Kastner, E. Karjalainen, G. N. Newton and V. Sans, *Adv. Mater.*, 2018, **30**, 1800159.

36 A. R. Schultz, P. M. Lambert, N. A. Chartrain, D. M. Ruohoniemi, Z. Zhang, C. Jangu, M. Zhang, C. B. Williams and T. E. Long, *ACS Macro Lett.*, 2014, **3**, 1205–1209.

37 J. Dupont and J. D. Scholten, *Chem. Soc. Rev.*, 2010, **39**, 1780–1804.

38 J. Guo, Q. Xu, Z. Zheng, S. Zhou, H. Mao, B. Wang and F. Yan, *ACS Macro Lett.*, 2015, **4**, 1094–1098.

39 A. Muñoz-Bonilla and M. Fernández-García, *Eur. Polym. J.*, 2018, **105**, 135–149.

40 A. Misra, I. Franco-Castillo, D. P. Müller, C. González, S. Eyssautier-Chuine, A. Ziegler, J. M. de la Fuente, S. G. Mitchell and C. Streb, *Angew. Chem., Int. Ed.*, 2018, **57**, 14926–14931.

41 M. D. T. Torres, S. Voskian, P. Brown, A. Liu, T. K. Lu, T. A. Hatton and C. de la Fuente-Nunez, *ACS Nano*, 2021, **15**, 966–978.

42 D. K. Bhui, H. Bar, P. Sarkar, G. P. Sahoo, S. P. De and A. Misra, *J. Mol. Liq.*, 2009, **145**, 33–37.

43 K. Ikemura, K. Ichizawa, M. Yoshida, S. Ito and T. Endo, *Dent. Mater. J.*, 2008, **27**, 765–774.

44 A. Heilmann, *Polymer Films with Embedded Metal Nanoparticles*, Springer-Verlag Berlin Heidelberg, Berlin, Germany, 2003.

45 S. V. Calderon, R. E. Galindo, N. Benito, C. Palacio, A. Cavaleiro and S. Carvalho, *J. Phys. D: Appl. Phys.*, 2013, **46**, 325303.

46 K. P. Menard and N. R. Menard, in *Encyclopedia of Polymer Science and Technology*, ed. H. F. Mark, Wiley, 4th edn, 2015, DOI: 10.1002/0471440264.pst102.pub2.

47 C. W. Duan, J. You, B. Liu, J. L. Ma, H. P. Zhou, H. B. Zhang and J. Zhang, *New J. Chem.*, 2018, **42**, 12243–12255.

48 B. Jamehbozorg and R. Sadeghi, *J. Chem. Eng. Data*, 2018, **63**, 331–340.

49 R. S. Datta, S. M. Said, S. R. Shahrir, N. Abdullah, M. F. M. Sabri, S. Balamurugan, Y. Miyazaki, K. Hayashi, N. A. Hashim, U. Habiba and A. M. Afifi, *RSC Adv.*, 2015, **5**, 48217–48223.

50 J. Jancar, J. F. Douglas, F. W. Starr, S. K. Kumar, P. Cassagnau, A. J. Lesser, S. S. Sternstein and M. J. Buehler, *Polymer*, 2010, **51**, 3321–3343.

51 J. Yue, P. Zhao, J. Y. Gerasimov, M. van de Lagemaat, A. Grotenhuis, M. Rustema-Abbing, H. C. van der Mei, H. J. Busscher, A. Herrmann and Y. Ren, *Adv. Funct. Mater.*, 2015, **25**, 6756–6767.

52 M. D. T. Torres, S. Sothiselvam, T. K. Lu and C. de la Fuente-Nunez, *J. Mol. Biol.*, 2019, **431**, 3547–3567.

53 A. Valls, J. J. Andreu, E. Falomir, S. V. Luis, E. Atrián-Blasco, S. G. Mitchell and B. Altava, *Pharmaceuticals*, 2020, **13**, 482.